Enhancing Resolution and Contrast in Second-Harmonic Generation Microscopy Using an Advanced Maximum Likelihood Estimation Restoration Method

[a]Mayandi Sivaguru†*, [b]Mohammad M. Kabir†, [c]Manas Rangan Gartia†, [d]David S. C. Biggs†, [e]Barghav S. Sivaguru, [e]Vignesh A. Sivaguru, [f]Zachary T. Berent, [f,a]Amy J. Wagoner Johnson, [a]Glenn A. Fried, [g]Gang Logan Liu, [h]Sakthivel Sadayappan and [f]Kimani C. Toussaint, Jr.

[a]Microscopy and Imaging Core Facility, Zeiss Microscopy Labs, Carl R. Woese Institute for Genomic Biology, University of Illinois at Urbana- Champaign, Urbana, IL, 61801, USA
[b]Department of Electrical and Computer Engineering and Bioengineering, University of Illinois at Urbana Champaign, Urbana, IL, USA
[c]Department of Mechanical and Industrial Engineering, Louisiana State University, Baton Rouge, LA3, USA
[d]KB Imaging Solutions LLC, 3849 Val Verde Rd, Loomis, CA 95650 USA
[e]College of Liberal Arts and Sciences, University of Illinois at Urbana- Champaign, Urbana, IL, USA
[f]Department of Mechanical Science and Engineering, University of Illinois at Urbana Champaign, Urbana, IL, USA
[g]Micro and Nanotechnology Lab, Department of Electrical and Computer Engineering, University of Illinois at Urbana- Champaign, Urbana, IL, USA
[h]Department of Internal Medicine, Heart, Lung and Vascular Institute, Division of Cardiovascular Health and Disease, College of Medicine, University of Cincinnati, Cincinnati, OH, USA
†Authors contributed equally
*Corresponding author

ABSTRACT

Second-harmonic generation (SHG) microscopy is a label-free imaging technique to study collagenous materials in extracellular matrix environment with high resolution and contrast. However, like many other microscopy techniques, the actual spatial resolution achievable by SHG microscopy is reduced by out-of-focus blur and optical aberrations that degrade particularly the amplitude of the detectable higher spatial frequencies. Being a two-photon scattering process, it is challenging to define a point spread function (PSF) for the SHG imaging modality. As a result, in comparison with other two-photon imaging systems like two-photon fluorescence, it is difficult to apply any PSF-engineering techniques to enhance the experimental spatial resolution closer to the diffraction limit. Here, we present a method to improve the spatial resolution in SHG microscopy using an advanced maximum likelihood estimation (AdvMLE) algorithm to recover the otherwise degraded higher spatial frequencies in an SHG image. Through adaptation and iteration, the AdvMLE algorithm calculates an improved PSF for an SHG image and enhances the spatial resolution by decreasing the full-width-at-half-maximum (FWHM) by ~20%. Similar results are consistently observed for biological tissues with varying SHG sources, such as gold nanoparticles and collagen in porcine feet tendons. By obtaining an experimental transverse spatial resolution of ~400 nm, we show that the AdvMLE algorithm brings the practical spatial resolution closer to the theoretical diffraction limit. Our approach is suitable for adaptation in micro-nano CT and MRI imaging, which has the potential to impact diagnosis and treatment of human diseases.

Keywords: Second Harmonic Generation, Porcine feet tendon, Advanced Maximum Likelihood Estimation, Restoration Method

*sivaguru@illinois.edu; phone 1 217 778-2423; fax 1 217 244-2496; http://www.igb.illinois.edu/core

1. INTRODUCTION

The optical resolution of light microscopy is fundamentally limited by Abbe and Rayleigh's limit [1]. New near-field (NSOM, TIRFM) and far-field (CLSM, 3D-SIM, Airyscan, STED, PALM/STORM) microscopy methods overcome this limit through tailored illumination, non-linear responses of fluorophore or through precise localization of the single molecule [2, 3]. To-date, there have been limited attempts at improving second-harmonic generation (SHG) microscopy image contrast and resolution [4, 5].

SHG imaging has been applied to differentiate different stages of cancers in breast, ovary, and skin tissues, evaluating fibrosis of liver, and kidney, delineating normal and diseased states of osteogenesis, Sjogren's syndrome, and stroma of cornea; and for quantitative analysis of tendon structural integrity in chicken and in horses [6-12].

In this paper, we demonstrate SHG image resolution and contrast improvement by implementing an advanced custom developed restoration algorithm. Image deconvolution algorithms can be broadly classified into six categories: (1) no-neighbors methods, (2) neighboring methods, (3) linear methods such as inverse filtering, Weiner filtering, linear least square, Tikhonov filtering and non-linear iterative methods such as Janson-van Cittert algorithm, nonlinear least square, iterative constrained Tikhonov-Miller algorithm, Carrington algorithm, (5) statistical iterative methods such as maximum likelihood estimation methods, maximum a posteriori method, and (6) Blind deconvolution methods. Here we have used a custom developed advanced MLE algorithm (AdvMLE) available as part of Olympus cellSens CI deconvolution software. What this algorithm does is based on the initial PSF estimate, which is adaptively modified on-the-fly by the optical properties and supplied data set based on Richardson-Lucy (RL) algorithm [13-19].

2. METHOD

Frozen, whole porcine feet were obtained from the Meat Science Laboratory at the University of Illinois at Urbana-Champaign. No live animals were handled for this study. After thawing, the extensor *digitorum lateralis* tendon was dissected. The control sample tendon was stored in phosphate buffered saline (PBS). The treated sample was immersed in 50 U/ml collagenase (Sigma-Aldrich, St. Louis, MO) for 24 hours. Samples were rinsed in PBS and then frozen in Optimal Cutting Temperature Compound (PSL Lab Supplies, Vista, CA) at – 20° C. Longitudinal and transverse sections were cut 10-micron thick using a Leica CM3050 S Cryostat and stored at – 80° C. Immediately before imaging, samples were thawed, wetted with PBS, and mounted between two cover #1.5 cover glasses.

SHG microscopy of porcine tendons were performed as described before [10-12]. The SHG set up used a Zeiss LSM 710 system together with a tunable Ti:Sapphire laser source at a repetition rate of 80 MHz producing 70-fs pulses. We used 780 nm excitation wavelength together with a quarter wave plate to produce circular polarization from a plane polarized fundamental so that to gain isotropic images from all molecular orientations at a given focal plane. We have used a 760 nm dichroic beam splitter and the fundamental was focused using a 63x 1.4 NA Oil immersion objective in order to approach to the diffraction limit. We have used 100 nm gold nanoparticles dispersed on a #1.5 cover glass to check the backward SHG image integrity from a spherical object as opposed to fiber like object such as the collagen. The gold nanoparticles SHG images were also obtained from the backward propagated SHG modality using non-descanned detectors. The emission signals were passed to a 680 nm short pass filter to clean out the IR and the frequency doubled signals were collected using a 390/18-25 nm band pass filter all obtained from Semrock Inc. The signals were integrated using a point scanner on to a Hamamatsu R6357 multi-alkali photomultiplier tubes. The average power at the sample was around 3mW. All parameters such as pixel dwell time, detector gain and frame averaging were kept constant between multiple sections and samples and images were obtained from several or at same locations with varied imaging parameters.

3. EXPERIMENT

We collected images of porcine tendons, and 100 nm gold nanoparticles in either 512x512 or 1024x1024 pixels format with varying average pixel dwell times to test the impact of noise and the recovery and restoration impact. All images were taken in three dimensions using the Z stack feature of the Zen image acquisition program at optimal and oversampled at times to compare the spacing effect on collagen fiber recovery and restoration. Using all of these optical properties, the raw data was restored under 20 constrained iterations using the AdvMLE algorithm which is part of the Olympus cellSens CI deconvolution software and resulting images were optimally adjusted with min/max intensity

profiles using either the Zen program or in the Autoquant image analysis program. The full width at half maximum values were calculated for both 100 nm gold nanoparticles as described below in Sigma Plot.

Restoration of images is also called deconvolution to correct the out of focus blur, which is due to convolution which happens at the time of image formation in an optical system. In linear microscopy the point spread function describes the optical system's performance from sample to image which is captured by a camera or a detector. This function is mathematically modeled by an equation called convolution in which the microscopic image (*g*) is a result of a convolution (⊗) between the actual object (*f*) and the PSF (*h*), plus a noise component (*n*) that is Poisson distributed from photon counting statistics. The expression describes this is [16-19]

$$g = f \otimes h + n, \tag{1}$$

where each variable is a three dimensional volume of intensity values. The process of estimating the ground truth data (*f*) from the observation (*g*) is termed *restoration or deconvolution*. There are many approaches to achieving deconvolution and these may be single step filtering (linear) or iterative in nature (non-linear) [18]. One of the most common approaches is the Richardson-Lucy (RL) iterative algorithm [13-15] which is based on Maximum Likelihood Estimation (MLE) with a log-likelihood measure assuming Poisson distributed noise. The simplified log-likelihood (*log L*) can be written as [17] based on RL algorithm is

$$\log(L) = \sum g \cdot \log(r_k) - r_k, \tag{2}$$

where $r_k = f_k \otimes h$ is the re-blurred estimate calculated by convolving the k^{th} estimate of the ground truth image (*f*) with the known PSF (*h*). The basic RL iteration for restoring the image is [17]

$$\hat{f}_{k+1} = \hat{f}_k \cdot \left(h \star \frac{g}{r_k} \right), \tag{3}$$

where $\star$ is the correlation operator, and $\cdot$ is element-wise multiplication. As negative signals are not observed by detectors which are designated as zeroes, each iteration is guaranteed to preserve non-negativity of the image and the point spread function. In addition, the likelihood measure is also increased, and is maximized when $r_k = g$.

Additionally, the RL iterations are known to converge slowly, so there are a variety of methods for both reducing the noise amplification and increasing the speed of convergence [13-15, 20].

A further extension of the standard deconvolution method is that of *blind deconvolution or restoration* where the PSF can be estimated along with the image as stated above. Using the RL approach, this can be simply achieved by switching the image and PSF variables as indicated here [17]

$$\hat{h}_{k+1} = \frac{1}{\sum \hat{f}_k} \hat{h}_k \cdot \left(\hat{f}_k \star \frac{g}{r_k} \right). \tag{4}$$

The restored and raw data images were further processed in Image J (National Institutes of Health, Bethesda, MD), an open source program for Fast Fourier Transform (FFT) analysis in order to investigate the band width gain after the restoration procedures. The FFT images were thresholded (138 or 148 with the selection of dark background) to remove the background uniformly across all samples and to obtain the major frequencies. Then the AdvMLE processed FFT images were subtracted by the raw data frequencies pixel-by-pixel to get the actual bandwidth gain. The line intensity profiles were made to analyze the resolution improvement by drawing a line with a width of 13-14 microns in the same programs. Also to represent the actual theoretical resolution of the optical system using 0.61*lambda/NA, the resolution was calculated to be ~0.37-0.38 microns with the 780 nm excitation and either the 40x 1.2 NA C-Apochromat Water immersion objective or 1.4 NA 63x Oil immersion objective. This limit was drawn graphically on the FFT images using a circle to represent the resolution limit and to visually show the improved frequencies after AdvMLE restoration compared to the raw data. The line profiles are extracted using 1 pixel with line traces using the same Image J program and the actual graphs are made in Sigma Plot version 13 using the extracted values and the same program was also used to calculate the full-width at half maximum values for the 100 nm gold nanoparticles.

4. RESULTS AND DISCUSSION

SHG and FT-SHG analysis have recently gained popularity due to the label free nature of the techniques, having diagnostic application potential [6-10, 12]. Since SHG microscopy is a non-linear process [6, 21, 22] at the point of generating signals of double the frequency of incoming fundamental light. Our focus is on the formed image which is linearly integrated as any other image in linear microscopy using the photomultiplier tubes as point detectors in optical scanning microscopy [1, 23, 24]. However, one has to evaluate this very carefully, as there are no reliable standards for SHG microscopy, due to its scattering and anisotropic distribution of signal depending on the molecular orientation [6, 21, 25]. That is one of the reasons why we have used a quarter wave plate to produce a circular polarization of the fundamental laser, so that all the molecules in the azimuthal angles could be imaged to obtain an isotropic image [12]. We first performed these experiments with 100 nm gold nanoparticles in which the SHG images were obtained in the backward direction only, where the signal is inherently incoherent as it is not in-phase with the fundamental laser [10, 22].

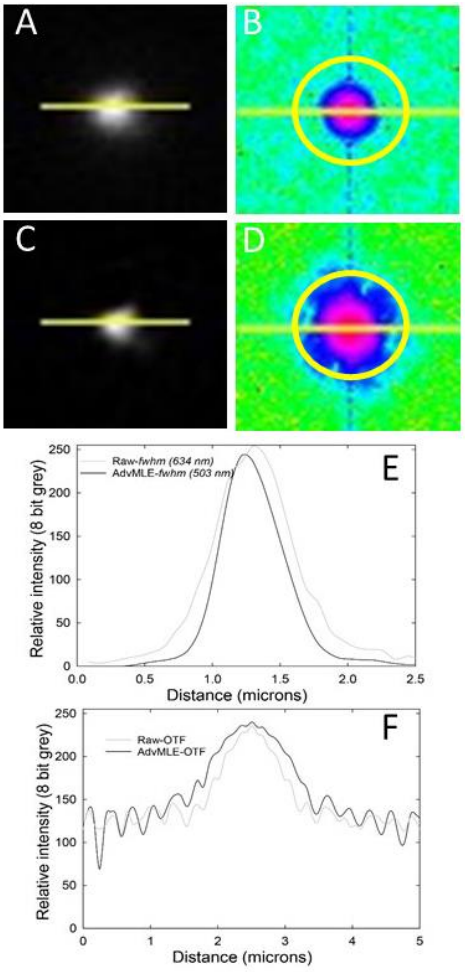

Figure 1. AdvMLE algorithm performance check using backward SHG images of 100 nm gold nanoparticles. The raw Z stack of the gold nanoparticle showed in maximum intensity distribution (A), and its corresponding Fourier transform with pseudo-colored look up table (B), the same particle after AdvMLE restoration (C and D). The yellow lines in A and C are used to trace the intensity distribution which is showed in E, with full width at half maximum values and the lines in B and D used to measure the optical transfer function performance between raw and AdvMLE from the FFT images and the traced values

are showed in F. The circles in B and D represents, 0.37 microns, which indicates the theoretical lateral resolution of the optical system. Scale bar 2.5 microns as indicated by the yellow trace lines in A and C.

Our investigation with gold nanoparticles yielded interesting results (Figure 1). First, we confirm the anisotropic nature of the SHG signal from the spherical shaped gold nanoparticles which could not be seen in raw data rather could be seen only in the AdvMLE processed data. This shape has been proposed for gold nanoparticle SHG before under various techniques either under simulation or experimentation [26]. The line intensity profiles before and after restoration of the gold nanoparticles showed ~20% improvement in the full-width half maximum of the peaks (Fig. 1E). In addition, we further analyzed the raw and AdvMLE processed images in Fourier space. These analyses showed that the AdvMLE processed image frequency distribution is closer to the theoretical resolution limit set by Abbe [1] for these modalities compared to raw data in which the frequencies are substantially lower. The trace of FFT images further affirmed the aforementioned statement, that the medium range frequencies close to the center and the high frequencies were substantially improved after the AdvMLE restoration (Fig. 1F). Such improvements of restoration algorithms on linear microscopy has been often used in the past [23, 27].

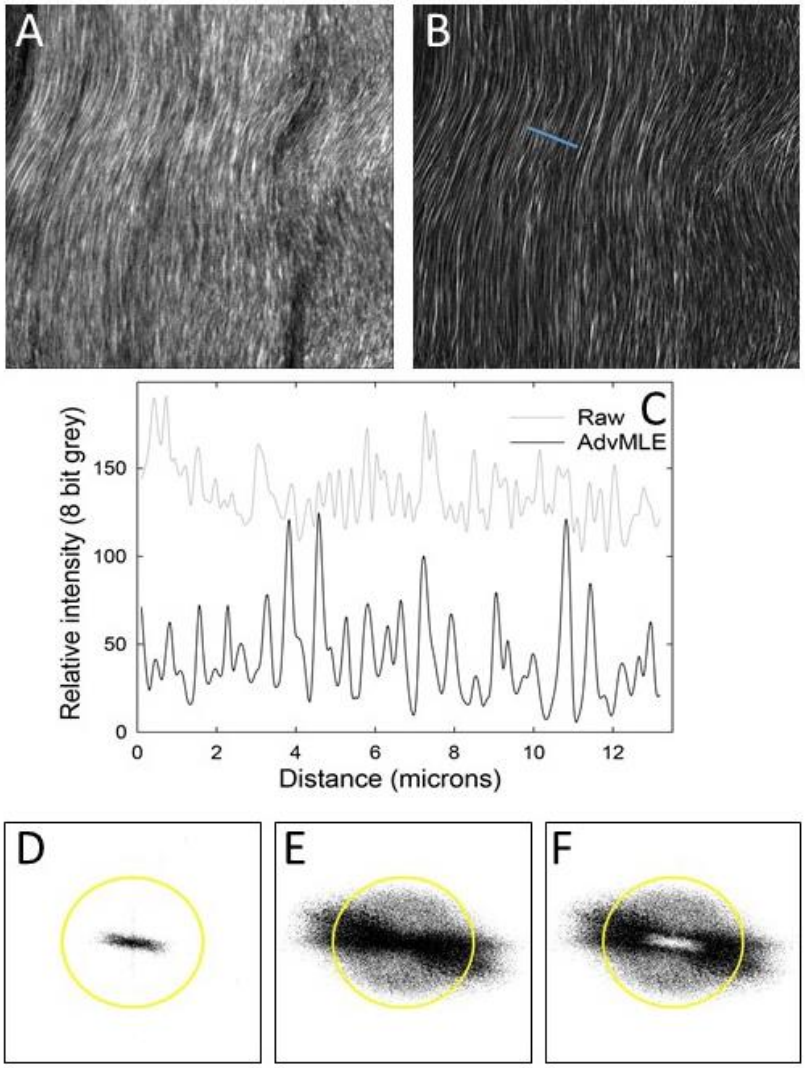

Figure 2. Enhanced resolution and contrast in SHG images of untreated porcine tendons. Raw data Z stack showing maximum intensity projection (A), the same image after AdvMLE restoration (B). The line in 'B' used to trace the signal improvement before and after AdvMLE processed images (comparing same Locations in A and B), is showed in C, D and E are Fourier transformed images of A and B respectively. Subtracted result of E-D showing the actual increase in bandwidth of AdvMLE processed images (F), showing higher orders of retrieved frequencies compared to raw data. The yellow circles in D-F

indicates the resolution frequency of 0.38 microns which is the Theoretical lateral resolution limit of the optical system. The line in B is ~13 microns which is also indicated by the X axis of the C.

In figure 2, a comparison (Fig 2 A and B) is provided between the raw data and AdvMLE restored 3D data of porcine tendon backward SHG images, showing substantial improvement in signal-noise ratio (SNR) of individual fibers, see the improved fiber signal to noise ratio (Fig 2 C). The improvement are seen both for samples processed with 512x512 or 1024x1024 pixel dimensions (data not shown), where the latter showed a better SNR and less pixilation due to the smaller pixel size [28]. The diffraction limited objective 63x Oil restored frequencies in all azimuthal directions and either filled the entire theoretical resolution limit or beyond (compare the circle) compared to the raw data (Fig. 2E and F) for the untreated tendons without collagenase treatment.

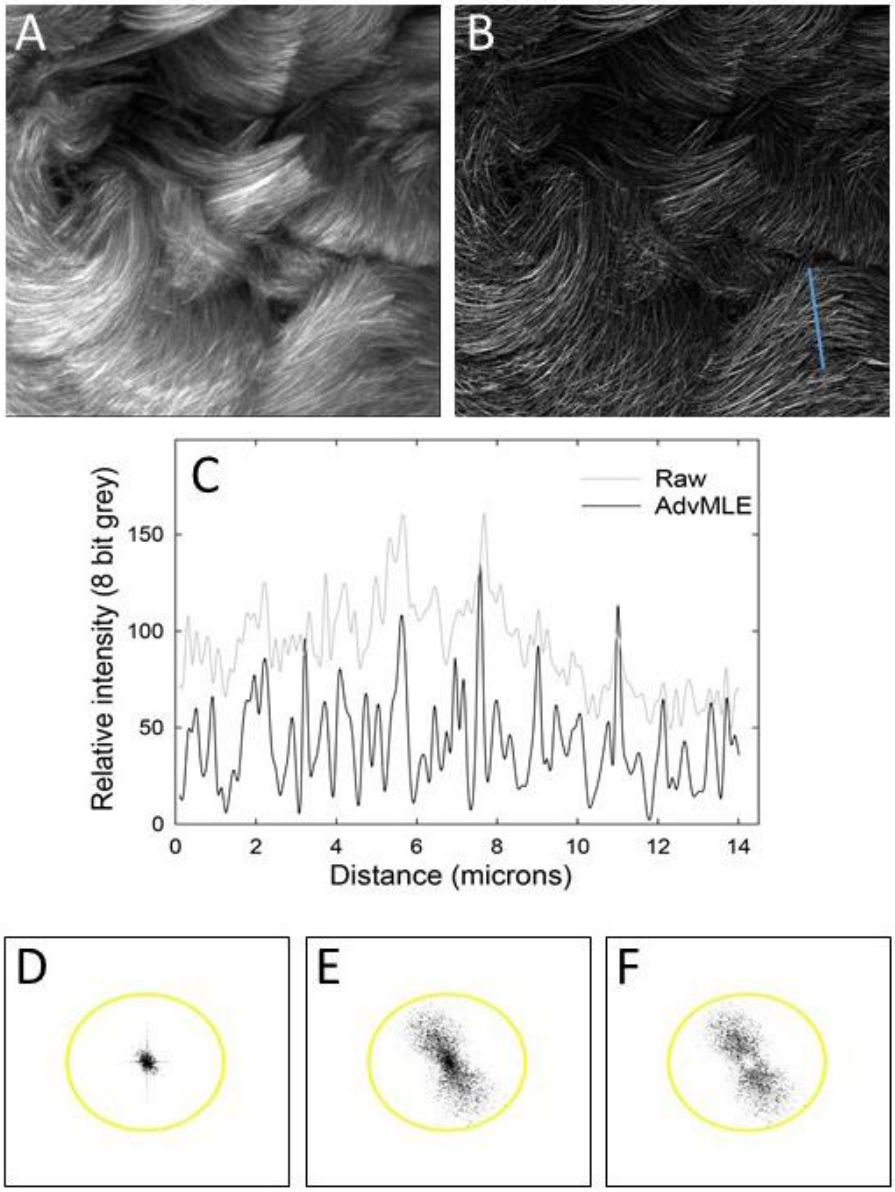

Figure 3. Enhanced resolution and contrast in SHG images of collagenase treated porcine tendons. Raw data Z stack showing maximum intensity projection (A), the same image after AdvMLE restoration (B). The line in 'B' used to trace the signal improvement before and after AdvMLE processed images (comparing same Locations in A and B), is showed in C, D and E

are Fourier transformed images of A and B respectively, and subtracted result of E-D showing the actual increase in bandwidth of AdvMLE processed images (F), showing higher orders of retrieved frequencies compared to raw data. The yellow circles in D-F indicates the resolution frequency of 0.38 microns which is the Theoretical lateral resolution limit of the optical system. The line in B is ~14 microns which is also indicated by the X axis of the C.

The results are presented from collagenase treated tendons in figure 3. The collagenase treatment overall damaged the integrity of the collagen, particularly the density and orientation. The collagenase treatment led to similar disorientations and higher angle spread *in vivo* in horse tendons [10-12]. Quantifying these differences is out of the scope of this paper, but we have extensively analyzed horse and chicken tendons previously using the Fourier transform-SHG technique [10-12]. Despite the use of the same objective and improved individual fiber signal to noise ratio as in untreated tendons (Fig. 3 A-C), the FFT analysis here showed that the restored frequencies are not as good as the untreated tendons. Between the raw and AdvMLE processed images the frequencies are higher, as in the untreated, but both the raw and processed images do not fill the diffraction limited resolution circle (Fig. 3 D-F). In addition, the frequencies do not exceed the circle at any given angle beyond the circle as in untreated. As per our observation in horse tendons, this may be due to the preferable damage to the fine fibers by the collagenase, detected in the backward propagated SHG signal. A useful future approach could be imaging using forward directed SHG together with backward SHG and performing a ratio metric analysis, which is expected to yield fruitful results [10-12]. Despite that the fine fibers are damaged but retaining thicker bundles shows the frequency gain in the lower and middle range of AdvMLE restored images. However, at the same time the fine fibers responsible for high frequency is selectively destroyed and hence the loss of high frequency signals in the FFTs of collagenase treated tendons compared to untreated [10-12, 22].

We have compared also tendons from chicken, sarcomere images from mouse heart and intact deep SHG images from unprocessed samples of chicken tendons, all yielding similar comparable results (data not shown) of improvement in resolution and contrast of SHG images ~20%. We believe this is substantial enough to visualize these structures at this resolution, rather than the visualizing un-restored noisy raw data for the purpose of disease diagnostics and treatment. Since the algorithm used created a point spread function adaptively based on the supplied data and imaging parameters, it could be applied elsewhere. For instance, this blind restoration could be applied to other modalities such as MRI and CAT Scan images where an optical systems point spread function could not be readily available as in the astronomical images or data sets.

5. ACKNOWLEDGMENT

All SHG imaging was performed at the Carl R. Woese Institute for Genomic Biology, Microscopy and Imaging Facility-Zeiss Microscopy Labs at the University of Illinois at Urbana-Champaign. This study is supported in part by NIH HL 105826 and HL 114749 (S.S), and the University of Illinois' Campus Research Board award for the LSM Objective Inverter (M.S., K.C.T.).

6. REFERENCES

[1] J. Pawley, "Fundamental Limits in Confocal Microscopy," Handbook of Biological Confocal Microscopy, Revised Edition, 15-26 (1989).

[2] S. W. Hell, S. J. Sahl, M. Bates *et al.*, "The 2015 super-resolution microscopy roadmap," Journal of Physics D-Applied Physics, 48(44), (2015).

[3] L. Schermelleh, R. Heintzmann, and H. Leonhardt, "A guide to super-resolution fluorescence microscopy," Journal of Cell Biology, 190(2), 165-175 (2010).

[4] N. Tian, L. Fu, and M. Gu, "Resolution and contrast enhancement of subtractive second harmonic generation microscopy with a circularly polarized vortex beam," Scientific Reports, 5, (2015).

[5] K. Korobchevskaya, C. Peres, Z. B. Li *et al.*, "Intensity Weighted Subtraction Microscopy Approach for Image Contrast and Resolution Enhancement," Scientific Reports, 6, (2016).

[6] P. Campagnola, "Second harmonic generation imaging microscopy: applications to diseases diagnostics," Anal Chem, 83(9), 3224-31 (2011).

[7] R. Ambekar, M. Chittenden, I. Jasiuk *et al.*, "Quantitative second-harmonic generation microscopy for imaging porcine cortical bone: comparison to SEM and its potential to investigate age-related changes," Bone, 50(3), 643-50 (2012).
[8] R. Ambekar, T. Y. Lau, M. Walsh *et al.*, "Quantifying collagen structure in breast biopsies using second-harmonic generation imaging," Biomed Opt Express, 3(9), 2021-35 (2012).
[9] T. Y. Lau, R. Ambekar, and K. C. Toussaint, "Quantification of collagen fiber organization using three-dimensional Fourier transform-second-harmonic generation imaging," Opt Express, 20(19), 21821-32 (2012).
[10] M. Sivaguru, S. Durgam, R. Ambekar *et al.*, "Quantitative analysis of collagen fiber organization in injured tendons using Fourier transform-second harmonic generation imaging," Opt Express, 18(24), 24983-93 (2010).
[11] M. Sivaguru, S. Durgam, R. Ambekar *et al.*, "Quantitative analysis of diseased horse tendons using Fourier-transform-second-harmonic generation imaging," Multiphoton Microscopy in the Biomedical Sciences Xi, 7903, (2011).
[12] M. Sivaguru, J. P. Eichorst, S. Durgam *et al.*, "Imaging horse tendons using multimodal 2-photon microscopy," Methods, 66(2), 256-267 (2014).
[13] L. B. Lucy, "An iterative technique for solving equations of statistical equilibrium," Monthly Notices of the Royal Astronomical Society, 326(1), 95-101 (2001).
[14] L. B. Lucy, "An iterative technique for the rectification of observed distributions," Astron. J., 79, 745 (1974).
[15] W. Richardson, "Bayesian-Based Iterative Method of Image Restoration," J. Opt. Soc. Am., 62(1), 55-59 (1972).
[16] D. S. C. Biggs, "Deconvolution of Fluorescence Microscope Imagery," Microscopy and Microanalysis, 15, 1528-1529 (2009).
[17] D. S. C. Biggs, "3D deconvolution microscopy," Current Protocols in Cytometry(SUPPL. 52), 12.19.1-12.19.20 (2010).
[18] D. S. C. Biggs, and M. Andrews, "Asymmetric iterative blind deconvolution of multiframe images," Advanced Signal Processing Algorithms, Architectures, and Implementations Viii, 3461, 328-338 (1998).
[19] D. S. C. Biggs, C. L. Wang, T. J. Holmes *et al.*, "Sub-pixel deconvolution of 3D optical microscope imagery," Advanced Signal Processing Algorithms, Architectures, and Implementations Xiv, 5559, 369-380 (2004).
[20] L. B. Lucy, "Iterative Technique for Rectification of Observed Distributions," Astronomical Journal, 79(6), 745-754 (1974).
[21] I. Freund, and M. Deutsch, "2nd-Harmonic Microscopy of Biological Tissue," Optics Letters, 11(2), 94-96 (1986).
[22] R. M. Williams, W. R. Zipfel, and W. W. Webb, "Interpreting second-harmonic generation images of collagen I fibrils," Biophysical Journal, 88(2), 1377-1386 (2005).
[23] M. Sivaguru, L. Mander, G. Fried *et al.*, "Capturing the Surface Texture and Shape of Pollen: A Comparison of Microscopy Techniques," Plos One, 7(6), (2012).
[24] M. Sivaguru, M. A. Urban, G. Fried *et al.*, "Comparative performance of airyscan and structured illumination superresolution microscopy in the study of the surface texture and 3D shape of pollen," Microsc Res Tech, (2016).
[25] Z. L. Tang, D. Xing, and S. H. Liu, "Imaging theory of nonlinear second harmonic and third harmonic generations in confocal microscopy," Science in China Series G-Physics Astronomy, 47(1), 8-16 (2004).
[26] P. C. Ray, "Size and shape dependent second order nonlinear optical properties of nanomaterials and their application in biological and chemical sensing," Chem Rev, 110(9), 5332-65 (2010).
[27] A. Goldraij, K. Kondo, C. B. Lee *et al.*, "Compartmentalization of S-RNase and HT-B degradation in self-incompatible Nicotiana," Nature, 439(7078), 805-10 (2006).
[28] D. W. Cromey, "Avoiding twisted pixels: ethical guidelines for the appropriate use and manipulation of scientific digital images," Sci Eng Ethics, 16(4), 639-67 (2010).